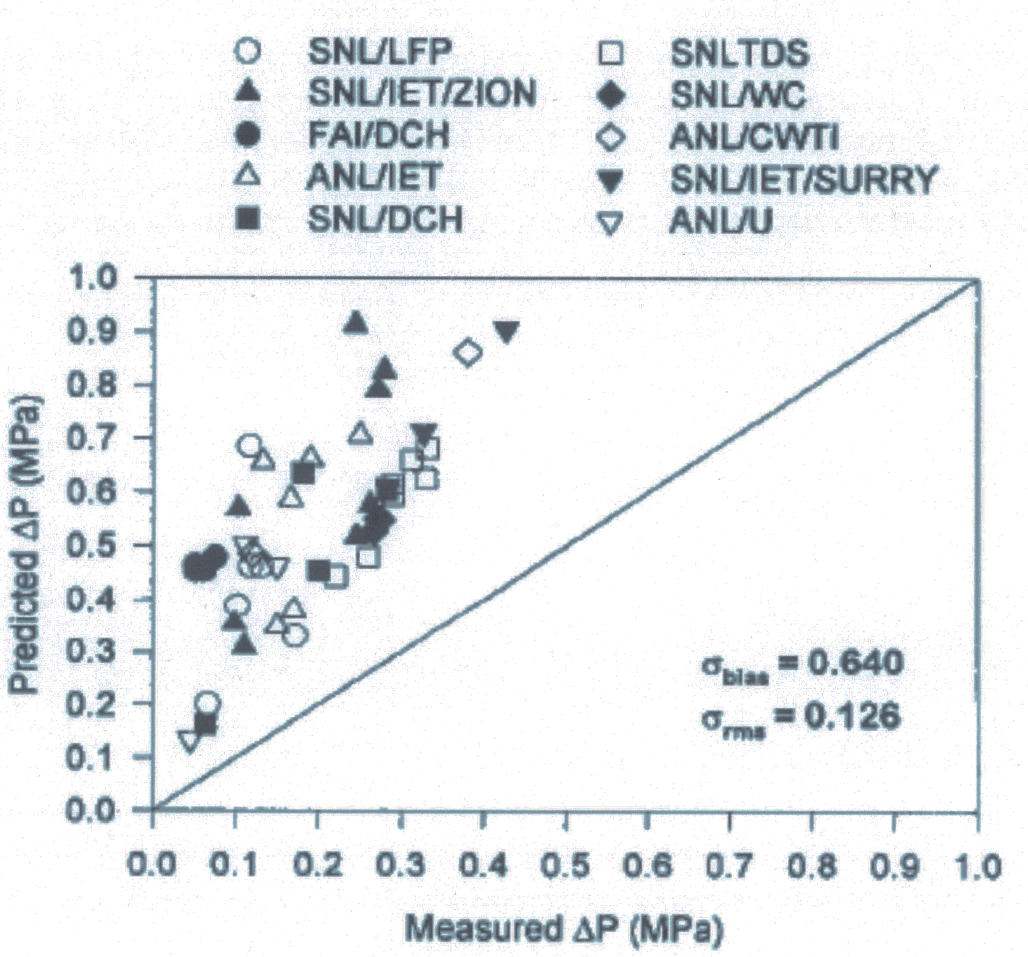

Figure 3-4 **Comparisons of pressure increase between SCE model and experiments.**

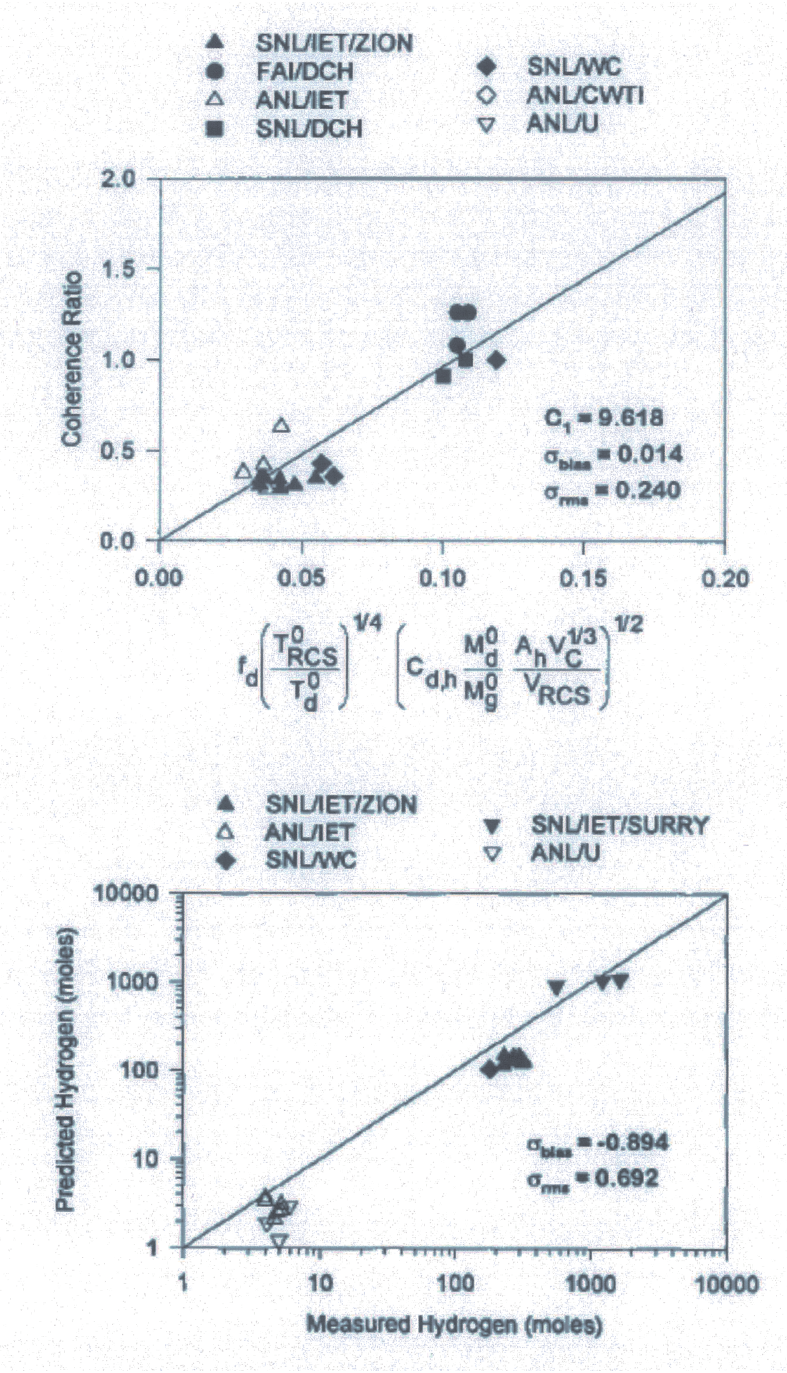

Figure 3-5 **Comparison of coherence ratio and hydrogen generation between the model prediction and the experiment data.**

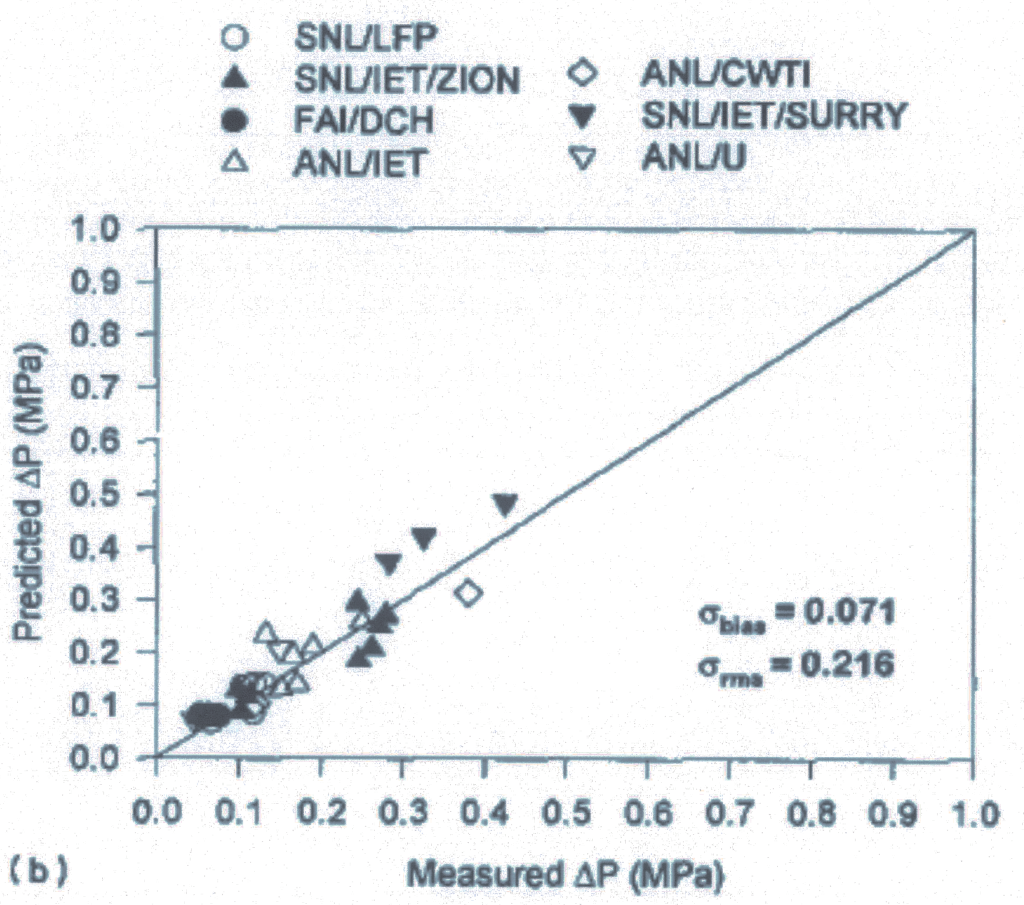

Figure 3-6 **Comparison of pressure increase between the model prediction and the experiment data.**

3.3 Modeling of Accident Scenarios

For the evaluation of DCH loads on the APR1400 containment, initial and boundary conditions were determined in advance, which include the APR1400 specific geometries of RCS and containment, the initial inventories of core materials, T/H condition of RCS and containment at the time of vessel breach (VB), the inventories of molten debris at VB and the characteristics of debris dispersal. Since DCH is possible only for high pressure sequences, appropriate scenarios had to be selected first.

Three scenarios were selected from the DCH studies of Zion (Reference 3) and Surry (Reference 5) where the efforts were consolidated into DCH issue resolution for Westinghouse and CE nuclear power plants. (Reference 4 and 6) These, designated as Scenario V, Va and VI in conformity with the references, simulated small break LOCAs with repressurization by operator intervention and were considered as conservative initiators in terms of DCH loads on the containment integrity. These scenarios will be described below in details.

Given an accident scenario, the initial and boundary conditions need to be prepared depend upon the DCH assessment methodology. For APR1400, two methodologies were used: the NUREG method and the mechanistic CONTAIN analysis. Whereas the NUREG method usually requires probabilistic distribution for major physical quantities, the CONTAIN analysis requires point-values for the same quantities. Moreover, the NUREG method requires plant-specific data from which it calculates related quantities internally. Thus, except for modeling-specific conditions required by each method, only general conditions are produced herein which can be classified in three subgroups: plant-specific information, quantification of initial conditions of molten corium in the lower plenum and thermo-hydraulic conditions, and quantification of the DCH phenomena. The bounding scenarios for DCH assessments are described as follows:

3.3.1 Scenario V (Va) - SBLOCA with Repressurization of RCS by Operator Intervention

Scenario V simulates a small break LOCA with repressurization of the RCS by operator intervention. It represents a core melt accident that progresses with water still present in the lower portions of the core. Such conditions lead to formation of a crust within the core followed by a massive release of melt when the crust fails. Accumulation of core material on the lower head of the RPV causes the lower head to heat up, eventually to the point where its structural strength is so degraded that it can no longer withstand the stresses induced in the lower head by elevated RCS pressures. Thus, creep rupture of the lower head is the expected failure mechanism.

Operator actions are assumed to repressurize the RCS to pressurizer safety valve opening setpoint. Operator intervention refills the RPV with water to the hot leg nozzles and quenches any steam remaining in the RCS to near saturation condition (~ 700 K). A non-condensible gas bubble prevents operators from refilling the entire RCS.

Consistent with TMI-II, the potential release of molten material to the lower head is controlled by the formation of a hemispherical crucible that excludes only the outer assemblies of the core. The outer assemblies are generally not in a severely degraded state because the RPV is flooded. Asymmetries in crucible growth ensure that localized penetration of the outer assembly and the core barrel would most likely occur when the crucible has grown (on average) to the outer assembly.

The containment conditions assume that active containment cooling systems (i.e., fan coolers or sprays) are not operational. However, the branch Scenario Va simulates the containment sprays in operation. It represents an accident in which the containment air temperature is very high and the steam mole fraction is very low to better envelop the range of containment conditions, so that the burning of hydrogen is highly likely. Even though these conditions are in the flammable regime, we do not guarantee that a random ignition source (unless intentional) will burn off the hydrogen prior to vessel failure even if the flammability limits are exceeded.

3.3.2 Scenario VI - SBLOCA Under Wet Core Conditions

Scenario VI simulates a small break LOCA with partial repressurization of the RCS by operator intervention. In the absence of any RCS leaks, hot leg failure would occur long before RV bottom head failure. These fully depressurize the RCS and are of no interest for DCH. Scenario VI can exist as the consequence of partial operator intervention that partially refills the RPV with water. Owing to the similarity in Scenarios V and VI, we emphasize only the differences in RCS pressure, RCS temperature and melt mass, with all other parameters developed in a manner similar to that for Scenario V.

The RCS gas at the time of vessel breach clearly must be superheated. In conjunction with the pressure and volume, the moles of gas in the RCS can be computed with the RCS temperature. The gas temperatures in each region of the RCS are estimated to be between 650K and 2800K. For this analysis, an average of 1,000K is assigned to this scenario. (Reference 3)

The potential release of molten material to the lower head is again controlled by the formation and failure of a crucible in the core region. Water occupies only the lowest regions of the core, so radial cooling of a growing crucible is reduced in this situation, and the crucible cold take on the bounding shape of an upright cylinder. We note that the molten pool must grow to the core boundary as a condition for core relocation, thus it shows some localized involvement of the outer assemblies. We expect, however, that asymmetries in crucible growth ensure that localized penetration of the outer assembly and core barrel would likely occur when the crucible has grown (on average) to the outer assembly. Consequently, the outer assemblies are excluded from our assessments.

4.0 DCH ANALYSIS IN APR1400

4.1 Melt Transport in Compartmentalized Containments

4.1.1 Cut-Off Droplet Size for Corium Deposition

Most reactor containments have many compartments so that the entrained melt drops will impinge and deposit on structures and walls which prevents efficient energy transport (thermal and chemical) from the cavity to the containment atmosphere. Assuming that all of the melt in the cavity is entrained by the vessel blowdown gas, the problem reduces to determining where the molten debris ultimately comes to rest, and how much of it was dispersed into the containment dome. The evaluation of debris transport can only be done on a plant by plant basis and here we focus our attention on the APR1400 containment geometry.

There are two main entrained corium transport paths from the cavity to the reactor dome: (i) through the annular gap between the reactor vessel and the cavity wall and (ii) through the cavity access area (i.e. staircase). While the flow up through the annular gap is redirected somewhat by neutron shield plugs and hot and cold legs, it will be conservatively assumed that all of the corium that enters the annular gap reaches the containment dome.

In order for the entrained corium to reach the cavity access staircase it must take a 90 degree turn in the cavity toward the sump. From the sump region it must turn upwards by 90 degrees to the corium chamber room. Then the entrained corium has to take another 90 degree turn toward the staircase. Finally the entrained corium has to take another 90 degree turn to flow up the staircase. Each 90 degree turn involves corium impingement on the wall that deflects the flow in the next lateral direction. Consider the first wall that deflects the flow, which is in the cavity itself.

As the flow approaches the wall it feels the presence of the solid surface and becomes deflected. Obviously, the gas component of the flow does not enter the wall but, instead, is completely deflected by the surface. As the droplets move with the gas, their paths will deviate from the gas streamlines because of droplet inertia and drag force and possibly because of gravity and Brownian motion if the droplets are small (< 1.0 μm). Here we assume that the droplets are large enough so that only droplet inertia and drag determine the droplet trajectories in the vicinity of the wall. The trajectories of the droplets in the flow deflection region are similar to the trajectories of the droplets in an inertial impactor, which consists of a particle/gas flow through a nozzle aimed at an impactor plate. Thus if the outer streamline of the flow (the effective width W of the wall) is replaced by an imaginary nozzle of inside radius W, calculated or experimental results for the droplet removal efficiencies of inertial impactors can be applied to estimate the droplet capture efficiency of the cavity wall during the HPME.

The most comprehensive numerical study of particle motion in an inertial impactor was performed by Marple (Reference 37, 38, and 39). Their numerical results for a circular impactor are well represented by the following correlations for the cut-off Stokes number St_{cut} or cut-off particle (or droplet) diameter D_{cut}:

$$St_{cut} = \frac{\rho_c \, D_{cut}^2 \, u_n}{9 \, \mu_g \, d_n} = 0.24 \tag{4-1}$$

where μ_g is the gas viscosity, ρ_c is the density of the liquid drop material (corium), d_n is the nozzle diameter, u_n is the nozzle gas velocity, and D_{cut} is the droplet diameter below which the droplets do not deposit on the impactor plate (or cavity wall in the present application). Equation (4-1) is in good quantitative agreement with the experimental data of Mercer and Stafford (Reference 40).

To use Eq. (4-1) we choose an imaginary nozzle in the flow deflection (or stagnation) region and we identify u_n and d_n with the oncoming two-phase corium/gas flow velocity $u_{2\phi}$ through the cavity toward the wall and with the effective width of the wall W. Therefore, Eq. (4-1) for the cut-off droplet diameter becomes

$$D_{cut} = 1.47 \left(\frac{\mu_g \, W}{\rho_c \, u_{2\phi}} \right)^{1/2} \tag{4-2}$$

Yuu and Jotaki (Reference 41) apparently were the first to suggest that the central part of an actual impactor nozzle can be regarded as a stagnation flow. Chiang (Reference 42) used this idea (Eq. 4-2) to predict water droplet deposition from a flashing jet impinging onto a plate. The next step in the analysis is the calculation of the two-phase flow velocity in the cavity.

4.1.2 Cavity Pressure and Two-Phase Flow Velocity

We consider the period in the direct containment heating transient in which all of the molten corium in the lower head has been displaced to the cavity by the in-vessel high pressure steam. While the pressure in the cavity P_{cav} is high it is assumed to be sufficiently below the vessel pressure P_0 so that the steam flow $\dot{m}_g \; (\text{in kg s}^{-1})$ from the vessel to the cavity is given by the critical flow equation:

$$\dot{m}_g = 0.61 \, A_0 \sqrt{P_0 \rho_{g,0}} \tag{4-3}$$

where A_0 is the area of the vessel failure opening and $\rho_{g,0}$ is the in-vessel steam density. The numerical coefficient 0.61 corresponds to isothermal critical flow. The choked two-phase corium/steam flow $\dot{m}_{2\phi}$ through the cavity cross-section toward the sump is

$$\dot{m}_{2\phi} = C_0 A_{cav} \sqrt{P_{cav} \rho_{2\phi}} \tag{4-4}$$

where A_{cav} is the cross-sectional flow area in the cavity, $\rho_{2\phi}$ is the two-phase density of the corium/steam mixture that occupies the cavity and the annular region and C_0 is a numerical constant whose value depends on the steam volume (void) fraction α in the two phase mixture and whether the flow is frozen (steam is thermally insulated from the corium) or the steam and corium are in thermal equilibrium (Reference 43).

The density of the two-phase mixture in the cavity region is

$$\rho_{2\phi} = \alpha\rho_g + (1 - \alpha)\,\rho_c \tag{4-5}$$

where ρ_g is the steam density in the cavity region and ρ_c is the density of the molten corium. Since $\alpha\rho_g << (1 - \alpha)\,\rho_c$, Eq. (4-5) may be simplified to

$$\rho_{2\phi} \cong (1 - \alpha)\,\rho_c \tag{4-6}$$

Turning our attention to the value of α, the volume of the cavity is denoted by the symbol V_{cav}. The portion of this volume occupied by the corium is

$$V_c = \frac{m_c}{\rho_c} \tag{4-7}$$

where m_c is the total mass of corium ejected from the vessel. The fraction of the total volume (V_{cav}) occupied by steam is then

$$\alpha = 1 - \frac{V_c}{V_{cav}} = 1 - \frac{m_c}{\rho_c V_{cav}} \tag{4-8}$$

We will also need to know the steam quality (mass fraction Y) in the cavity and annular regions. The quality is related to α by the formula

$$Y = \frac{\rho_g \alpha}{\rho_g \alpha + (1 - \alpha)\rho_c} \cong \frac{\rho_g}{\rho_c}\left(\frac{\alpha}{1 - \alpha}\right) \tag{4-9}$$

From the ideal gas law the density of the steam in the cavity is

$$\rho_g = \frac{P_{cav} M_g}{R_{id} T_0} \tag{4-10}$$

where M_g is the molecular weight of the steam, R_{id} is the ideal gas constant and T_0 is the temperature of the steam in the cavity. The subscript "0" signifies that T_0 is also identified with the steam temperature in the vessel since frozen two-phase flow is assumed.

The steam mass flow through the annular gap is assumed to be small compared with that through the cavity. This assumption will be justified by the result of the analysis. It follows that the steam mass flow rate through the cavity must match the steam mass flow rate from the vessel; therefore

$$Y\dot{m}_{2\phi} = \dot{m}_g \tag{4-11}$$

Combining Eqs. (4-3), (4-4), (4-6), (4-9), (4-10) and (4-11) and solving the result for P_{cav} gives

$$P_{cav} = \left(\frac{0.61\, A_0 R_{id} T_0}{M_g C_0 A_{cav}} \right)^{2/3} \left[\frac{P_0 \rho_{g,0} \rho_c (1-\alpha)}{\alpha^2} \right]^{1/3} \quad (4\text{-}12)$$

The reactor operating pressure is about P_0 = 1.7 x 10^7 Pa. The steam in the vessel is assumed to be superheated to T_0 = 1000 K. From the ideal gas law $\rho_{g,0}$ = 36.8 kg m^{-3}. We assume that m_c = 97.5 x 10^3 kg of corium is ejected from the reactor vessel and that the density of corium $\rho_c \cong$ 9250 kg m^{-3}. The volume of the APR1400 cavity is V_{cav} = 368 m^3. Therefore, from Eq. (4-8) α = 0.971. From the choked flow charts in reference 43, for α = 0.971 and the assumption of frozen flow, $C_0 \equiv$ 0.6. The flow area in the cavity is A_{cav} = 21.8 m^2. The failure area can be calculated through modeling the ablation of reactor vessel wall when the corium is ejected by the high pressure. TCE model calculations were performed to show that the diameter of the failure in the vessel wall can be as large as 0.5 m, corresponding to a failure area of 0.2 m^2. The cavity pressure is, from Eq. (4-12),

$$P_{cav} = 1.48 \times 10^6 \text{ Pa} \quad (4\text{-}13)$$

The two-phase flow velocity toward the cavity wall that deflects the flow is, from Eqs. (4-4) and (4-6)

$$u_{2\phi} = \frac{\dot{m}_{2\phi}}{\rho_{2\phi} A_{cav}} = C_0 \sqrt{\frac{P_{cav}}{\rho_c (1-\alpha)}} = 44.9\, \text{m s}^{-1} \quad (4\text{-}14)$$

4.1.3 Fraction of Drops that Impinge on the Wall

Post-DCH-test measurements of particle sizes with sieves have shown that particles are distributed lognormally with a mass median diameter $\bar{D}$ of approximately 0.5 mm and a geometric standard deviation $\sigma_g \cong$ 4.0 (Reference 5, 20 and 44). For a log-normal distribution the fraction F of the total mass of particles with diameters less than D_{cut} are

$$F = \frac{1}{2} - \frac{1}{2} \text{erf} \left[-\frac{1}{\sqrt{2} \ln \sigma_g} \ln \left(\frac{D_{cut}}{\bar{D}} \right) + \frac{3}{2\sqrt{2}} \ln \sigma_g \right] \quad (4\text{-}15)$$

Inserting $u_{2\phi}$ = 44.9 m s^{-1} (Eq. 4-14), μ_g = 3.55 x 10^{-5} kg m^{-1} s^{-1} (for H_2O at 1000 K), ρ_c = 9250 kg m^{-3} and W $\cong$ 5.0 m for the effective width of the cavity wall into Eq. (4-2) gives

$$D_{cut} = 3.04 \times 10^{-5} \text{ m} \quad (4\text{-}16)$$

From Eq. (4-15) we get

$$F = \frac{1}{2} - \frac{1}{2} \text{erf}(2.9) = 2.05 \times 10^{-5} \quad (4\text{-}17)$$

for the fraction of corium drops that are not captured by the wall. While it is likely that a higher mass fraction of droplets than this escapes the cavity the calculation does show that most of the

melt that flows toward the entrance to the corium chamber room deposits on the cavity wall. The corium melt film on the wall drains to the cavity floor only to be re-entrained again and cycled back to the wall. Note that re-entrainment of melt from the surface of the liquid film on the wall is unlikely since the instability of the Kelvin-Helmholtz type is bounded in stagnation counter flow fields (Reference 45).

4.1.4 Fraction of Entrained Melt Transported Through Reactor Vessel Annulus

The two-phase corium/steam flow through the reactor vessel annulus obeys the same equation as that for flow through the cavity, namely Eq. (4-4) with A_{cav} replaced by the cross-sectional flow area A_{an} in the annulus:

$$\dot{m}_{2\phi} = C_0 \, A_{an} \sqrt{P_{cav} \, \rho_{2\phi}} \tag{4-18}$$

Thus the fraction of the dispersed corium that enters the containment dome via the reactor annulus is

$$f_{dom} = \frac{A_{an}}{A_{cav} + A_{an}} \tag{4-19}$$

This fraction represents all of the corium that enters the containment dome since we just demonstrated that practically all of the corium that travels towards the compartments will be trapped. For the ARP1400 containment A_{an} = 1.96 m^2 and A_{cav} = 21.8 m^2 and

$$f_{dom} = 0.082 \tag{4-20}$$

It should be mentioned that the NUREG/CR-6075 (Reference 35) analyzed a number of DCH experiments and concluded that Eq. (4-19) represents the debris flow through the annular gap.

A word of caution must be inserted here in that the predicted cavity pressure P_{cav} = 1.48 x 10^6 Pa (Eq. 4-13) exceeds the differential pressure of 7.5 x 10^5 Pa to fail the seal table. Whether or not the seal table fails depends on the instantaneous pressure in the containment dome and the pressure drop through the ICI chase from the reactor cavity to the seal table. However, even if the seal table is indeed failed, it is expected the opening is a gap-type of opening, instead of the line-of-sight pathway allowing the direct transport of corium to the open space of the containment. Also, for the flow to go through the path of the failed seal table, it must first impinge the wall at the end of the cavity and make a 90 degree (upward) turn to ICI chase chamber, where the seal table is located. The previous discussion has shown that nearly all the entrained corium will be captured by the impingement and very little corium will be released through the failed seal table.

4.2 DCH model for APR1400

DCH induced loads in APR1400 were calculated using the TCE model. In the calculations, three scenarios were considered which are described in NUREG/CR-6338 (Reference 46).

4.2.1 Generation of probabilistic distribution and sampling for uncertain input parameters

The high uncertain parameters considered in the TCE model are to be quantified as probability density functions. In this calculation, initial mass of UO_2 in melt at vessel breach, fraction of Zr oxidized, coherence ratio, containment fragility curve are selected as probabilistic input parameters. The initial mass of UO_2 in melt at vessel breach, the fraction of Zr oxidized and variations in the coherence ratio were quantified as probability density curves. For the TCE model analysis, each probabilistic input parameter is sampled using the LHS (Latin Hypercube Sampling) method. In this calculation, the 10,000 samples per each probabilistic input parameter are used.

4.2.2 Quantification of point input parameters

Referring to the specific design information of APR1400 and the initial and boundary conditions for selected scenarios, the point input parameters are quantified. In this calculation, the point input parameters are as follows:

- Lower head wall thickness (m)
- Lower plenum volume (m^3)
- Initial lower head hole diameter (m)
- Lower head wall temperature at VB (K)
- Mass of Control Rod Material in melt (metric ton)
- Mass of UO_2 in core (metric ton)
- Mass of Zr in core (metric ton)
- Mass of steel in lower plenum (metric ton)
- Reactor cavity specific multiplier in coherence ratio
- RCS pressure at VB (MPa)
- RCS volume (m^3)
- RCS temperature at VB (K)
- Containment pressure at normal operation (MPa)
- Containment temperature at normal operation (K)
- Containment pressure at VB (MPa)
- Containment temperature at VB (K)
- Containment free volume (m^3)
- Reactor cavity free volume (m^3)

- Fraction of debris remaining in subcompartment
- Volume fraction of subcompartment
- Auto-ignition temperature (K)
- Temperature of debris melt (K)
- Fraction of Zr block relocated
- Fraction of H_2 generated in RCS that stays in RCS
- Melt fraction ejected into the reactor cavity
- Fraction of ejected melt dispersed from reactor cavity

4.2.3 TCE calculation

The TCE calculation is performed to evaluate the DCH loads. The probabilistic and point input parameters are used to evaluate the equations. In each trial the calculated DCH pressure is compared against the failure pressure sampled from the containment fragility curve. The process is repeated 10,000 times and the number of cases where the DCH pressure exceeds the containment failure pressure is recorded. The number of “failed” cases divided by 10,000 gives the containment failure probability.

5.0 SUMMARY OF RESULTS FOR APR1400 DCH ANLAYSIS

DCH induced loads in APR1400 were calculated using the TCE model. In the calculations, three scenarios were considered which are similar to those considered in NUREG/CR-6338 (Reference 46). The initiation event of these scenarios is considered to be a small LOCA and re-pressurization of RCS due to operator's intervention. Scenario V and Va assume the RCS pressure before the vessel failure is at the pressurizer PORV set point of 17 MPa, and the water level in the RCS is high enough to cover the core region. The containment pressure for the scenario V is about 2.5 bar while the pressure for the scenario Va is about 1.25 bar. A corium pool in the shape of a hemisphere forms in the core region. Eventually the crust surrounding the pool fails and the corium is relocated into the lower plenum, where it causes the vessel failure. The amount of corium relocated into the lower plenum is assumed to follow a distribution with the maximum and best estimate about 81 tons and 40 tons respectively. Scenario VI assumes the RCS pressure before the vessel failure is at one half of the pressurizer set point, about 9 bars. The water level in the vessel covers only the lower portion of the core, and an upright cone shape of corium pool forms in the core region. The crust fails and the corium relocates into the lower plenum. The distribution of the mass of corium in the lower plenum has the maximum and best estimate values of about 98 tons and 49 tons respectively. Besides the mass of corium, several other parameters are assumed for each scenario to follow probabilistic distributions, including the containment failure pressure, fraction of Zr oxidation, and coherence time ratio in the TCE model.

Although most of the corium is expected to be captured by the wall at the end of the cavity, the calculations assume adjacent compartments around the cavity are capable of exchanging energy with the corium particle. The subcompartment in the TCE model is comprised of the cavity, corium chamber, ICI chase compartment, reactor cavity access area, and regenerative heat exchanger room. The total volume of these spaces is about 2% of the entire volume of the containment. The fraction of corium going directly into the containment upper dome is about 0.28, which is estimated based on the projected area of the reactor vessel, divided by the floor area of the cavity. The fraction is much more conservative than that estimated in the previous section based on the area fraction.

Based on the conservative assumptions described above, the loads (pressures) caused by DCH were compared with the containment failure pressure. Figure 5-1 shows the maximum pressure distributions for all three scenarios compared with the distributions of the containment failure pressure. As shown, there is only small pressure interval of intersection between the DCH pressures and the failure pressure (for the very high DCH pressure and very low containment failure pressure). The conditional probability of containment failure in DCH is estimated less than 0.1%, which, according to reference 46, can be considered as an acceptable risk.

TS

Figure 5-1 Comparison of pressures due to DCH and the containment failure pressure for APR1400.

6.0 CONCLUSIONS

An extensive database from integral tests on DCH has been developed over the last three decades. The database covers cavity designs with large instrument tunnels connected to subcompartments and cavity designs of the annular type where one of the paths to the containment is the annular space between the reactor and the vessel. The most important conclusions derived from these experiments are:

1. The containment pressure is limited significantly by the presence of compartments between the reactor cavity and the containment dome which prevent the transport of large quantities of fine, hot debris to the containment dome.

2. As a result of the compartmentalization mentioned above, the DCH containment pressures are not sufficient to challenge containment integrity for the plant types investigated.

3. A linear scaling approach to experiments at substantially different scales has been demonstrated to be valid for plants with compartmentalized geometry.

4. The hydrogen produced and burned during the DCH event contributes significantly to the containment pressure rise.

5. The experimental containment pressure rise results can be adequately correlated by considering the regions in the containment (e.g., the TCE model).

6. The experiments performed with water in the cavity and/or on the basement floor have not revealed a large effect of water on containment pressurization. However, significant cavity pressurization has been observed in some tests with water in the cavity.

While DCH experiments have not been directed towards examining the consequences of DCH occurring in the APR1400 reactor, significant DCH pressurization of the APR1400 containment is judged to be most unlikely. It has been well established by the DCH laboratory research that containment structures and compartments have a first order mitigating influence on the pressurization potential of DCH. The number of compartments between the cavity and the containment dome of the APR1400 reactor are not at all conducive to supporting a strong DCH event, as demonstrated in this report.

According to the NUREG/CR-6075 (Reference 35) methodology, the DCH issue is considered resolved if the containment failure probability due to DCH, obtained through a probabilistic evaluation of phenomenological analysis and its uncertainties, is found to be lower than a certain threshold value. The severe accident scenario that can lead to DCH in APR1400 is identified as a small LOCA with RCS re-pressurization due to operator intervention and three representative scenarios were considered.

For each of the three scenarios, zero (0) containment failure case has resulted from 10,000 trials. Based on this outcome, the CCFP in APR1400 due to DCH is estimated to be less than 0.01% (0.0001). This indicates that APR1400 meets the success criterion established in reference 46 for PWR large dry containment, where DCH problem is considered resolved if CCFP is less than 1%

(0.01).

7.0 REFERENCES

1. Commonwealth Edison Company (CECo), 1981, Zion Probabilistic Safety Study, Chicago, Illinois.
2. Nuclear Regulatory Commission (NRC), 1975, "Reactor Safety Study," WASH-1400.
3. Tarbell, W. W., et al., 1984, "High-Pressure Melt Streaming (HIPS) Program Plan," SAND82-2477, NUREG/CR-3025, Sandia National Laboratories.
4. Tarbell, W. W., et al., 1986, "Melt Expulsion and Direct Containment Heating in Realistic Plant Geometries," Proc. of the International ANS/ENS Topical Meeting on Thermal Reactor Safety, San Diego, California.
5. Tarbell, W. W., et al., 1986, "Pressurized Melt Ejection into Scaled Reactor Cavities," SAND86-0153, NUREG/CR-4512, Sandia National Laboratories.
6. Pilch, M. and Tarbell, W. W., 1986, "Preliminary Calculations on Direct Heating of a Containment Atmosphere by Airborne Core Debris," SAND85-2439, NUREG/CR-4455, Sandia National Laboratories.
7. Spencer, B. W., et al, 1983, "Corium/Water Dispersal Phenomena in Ex-Vessel Cavity Interactions," Paper TS-15.5, proc. Int'l. Mtg. on LWR Severe Accident Evaluation, Vol. 2, Cambridge, MA.
8. Spencer, B. W., et al., 1983b, "Overview and Recent Results of ANL/EPRI Corium/Water Thermal Interaction Investigations," Paper TS-15.2, Proc. Int'l. Mtg. on LWR Severe Accident Evaluation, Vol. 2, Cambridge, MA.
9. Spencer, B. W., et al., 1987, "Hydrodynamics and Heat Transfer Aspects of Corium-water Interactions," EPRI NP-5127, Argonne National Laboratory.
10. Spencer, B. W., et al., 1988, "Results of EPRI/ANL DCH Investigations and Model Development," ANS/ENS Conference on Thermal Reactor Safety, Avignon, France.
11. Tarbell, W. W., et al., 1987, "DCH Experiments and Analyses at Sandia National Laboratories," Containment Loads and Molten Core Containment Expert Opinion Meeting, Albuquerque, New Mexico.
12. Tarbell, W. W., et al., 1987, "Results from the DCH-I Experiment," SAND86-2483, NUREG/CR-4817, Sandia National Laboratory.
13. Tarbell, W. W., et al., 1988, "DCH-2: Results from the Second Experiment Performed in the Surtsey Direct Heating Test Facility," SAND87-0976, NUREG/CR-4917, Sandia National Laboratory.
14. Tarbell, W. W., et al., 1988, "Direct Containment Heating and Aerosol Generation During High-Pressure-Melt Expulsion Experiments," Trans. Am. Nucl. Soc., 57, 361.
15. Allen, M. D., et al, 1991, "Experimental Results of Direct Containment Heating by High-Pressure Melt Ejection Into the Surtsey Vessel: The DCH-3 and DCH-4 Tests," SAND90-2138, Sandia National Laboratory.

16. Marx, K. D., 1989, "A Computer Model for the Transport and Chemical Reaction of Debris in Direct Containment Heating Experiments," Nuclear Sci. & Eng., 102, 391-407.

17. Henry, R. E. , 1989, "An Evaluation of Fission Product Release Rates During Debris Dispersal," Proc. of the ANS/ENS Intl. Topical Mtg. on Probability, Reliability and Safety Assessment, Vol. 1, pp. 375-383.

18. Henry, R. E., et al., 1991, "Direct Containment Heating Experiments in a Zion-Like Geometry," AIChE Sym., Series, Vol. 87, No. 293, Heat Transfer - Minneapolis 1991, pp. 86-98.

19. Binder, J. L., et al., 1994, "Direct Containment Heating Integral Effects Tests at 1/40 Scale in Zion Nuclear Power Plant Geometry," Argonne National Laboratory, ANL-94/18, NUREG/CR-6168.

20. Allen, M. D., Pilch, M., Griffith, R. O. and Nichols, R. T., 1992, "Experimental to Investigate the Effect of Water in the Cavity on Direct Containment Heating (DCH) in the Surtsey Test Facility - The WC-I and WC-2 Tests," SAND91-1173, Sandia National Laboratories, Albuquerque, NM, March.

21. Allen, M. D., et al., 1992, "Quick-Look Report on the Second Integral Effects Tests (IET-2): Thermite Temperature Measurements," Sandia National Laboratories.

22. Allen, M. D., Blanchat, T. K., Pilch, M. and Nichols, R. T., 1992, "The Effects of Condensate Levels of Water on Direct Containment Heating (DCH) in Zion-like Geometry: The Fourth Integral Effects Test (IET-4) Conducted in the Surtsey Test Facility," SAND92-1241, Sandia National Laboratories, Albuquerque, NM, September.

23. Allen, M. D., Blanchat, T. K., Pilch, M. and Nichols, R. T., 1992, "Experimental Results of an Integral Effects Test in a Zion-like Geometry to Investigate the Effects of a Classically Inert Atmosphere on Direct Containment Heating: The IET-5 Experiment," SAND92-1623, Sandia National Laboratories, Albuquerque, NM, November.

24. Allen, M. D., et al., 1992, "Quick-Look Report on the Sixth Integral Effects Test (IET-6) in the Surtsey Test Facility," Sandia National Laboratory.

25. Allen, M. D., Blanchat, T. K., Pilch, M. and Nichols, R. T., 1992, "An Integral Effects Test to Investigate the Effects of Condensate Levels of Water and Preexisting Hydrogen on Direct Containment Heating in the Surtsey Test Facility: The IET-7 Experiment," SAND92-2021, Sandia National Laboratories, Albuquerque, NM, December.

26. Allen, M. D., Blanchat, T. K., Pilch, M. and Nichols, R. T., 1993, "Experiments to Investigate the Effects of Fuel/Coolant Interactions on Direct Containment Heating - The IET-8A and IET-8B Experiments," SAND92-2849, Sandia National Laboratories, Albuquerque, NM, February.

27. Allen, M. D., et al., 1994, "Experiments to Investigate Direct Containment Heating Phenomena with Scaled Models of the Zion Nuclear Power Plant in the SURTSEY Test Facility," Sandia National Laboratory, SAND93-1049, NUREG/CR-6044.

28. Ishii, M., Revankar, S. T., Zhang, G., Wu, Q. and O'Brien, P., 1994, "Air-Water Simulation of Phenomena of Corium Dispersion and Direct Containment Heating," NUREG/CR-6267, PU NE-93-1.

29. Zhang, G. J. and Ishii, M., 1995, "Entrance Effect on Droplet Entrainment in DCH," ANS Proceedings, HTC-Volume 8, 1995 National Heat Transfer Conference, Portland, Oregon, pp. 375-383.

30. Hammersley, R. J. et al., 1995, "Direct Containment Heating Experiments for Vandellos and Asco Nuclear Power Plants," ANS Proceedings, Vol. 8, pp. 384-392, 1995 National Heat Transfer Conference, Portland, OR.

31. Blanchat, T. K., et al., 1994, "Experiments to Investigate Direct Containment Heating Phenomena with Scaled Models of the Surry Nuclear Power Plant," Sandia National Laboratories, SAND93-2519, NUREG/CR-6152.

32. Blanchat, T. K., Pilch, M. M. and Allen, M. D., 1997, "Experiments to Investigate Direct Containment Heating Phenomena with Scaled Models of the Calvert Cliffs Nuclear Power Plant," NUREG/CR-6469, SAND96-2289, Sandia National Laboratories, Albuquerque, NM.

33. Blanchat, T. K., et al., 1999, "Direct Containment Heating Experiments at Low Reactor Coolant System Pressure in the Surtsey Test Facility," NUREG/CR-5746, SAND99-1634, Sandia National Laboratories, Albuquerque, NM.Meyer, L., Albrecht, G., Caroli, C. and Ivanov, I., 2009, "Direct Containment Heating Integral Effects Tests in Geometries of European Reactors," Nucl. Engng. & Design 239, pp. 2070-2084.

34. Pilch, M. M., Yan, H. and Theofanous, T. G., 1994, "The Probability of Containment Failure by Direct Containment Heating in Zion," NUREG/CR-6075, SAND93-1535, Sandia National Laboratory, Albuquerque, NM.

35. Pilch, M. M., 1996, “A Two-Cell Equilibrium Model for Predicting Direct Containment Heating,” Nuclear Engineering and Design, Vol. 164, p.61~94.

36. Marple, V. A., 1970, "A Fundamental Study of Inertial Impactors," PhD. Thesis, University of Minnesota, Minneapolis, MN.

37. Marple, V. A. and Liu, B. Y. H., 1974, "Characteristics of Laminar Jet Impactors," Environmental Sci. and Tech. 8, pp. 648-654.

38. Marple, V. A. and Rubow, K. L., 1986, "Theory and Design Guidelines," In Cascade Impactor Sampling and Data Analysis, American Industrial Hygiene Association Monograph, J. P. Lodge and T. L. Chan (editors), pp. 79-101.

39. Mercer, T. T. and Stafford, R. G., 1969, "Impaction from Round Jets," Annals Occupation Hygiene 12, pp. 41-48.

40. Yuu, S. and Jotaki, T., 1978, "The Calculation of Particle Deposition Efficiency Due to Inertia, Diffusion and Interception in the Plane Stagnation Flow," Chem. Engng, Sci. 33, pp. 971-978.

41. Chiang, H. W., 1983, "A Model for the Removal of Water Droplet Aerosols from a Flashing Jet Impinging Onto a Plate," Presented at OECD/CSNI Specialist Meeting Nuclear Aerosols in Reactor Safety, Cologne, Germany (June 15-18).

42. Leung, J. C. and Epstein, M., 1990, "A Generalized Correlation for Two-Phase Nonflashing Homogeneous Choked Flow," J. Heat Transfer 112, pp. 528-530.

43. Allen, M. D., et al., 1994, "Test Results on Direct Containment Heating by High-Pressure Melt Ejection into the Surtsey Vessel: the TDS Test Series," Sandia National Laboratories Report, SAND91-1208.

44. Erickson, G. G. and Olfe, D. B., 1978, "Growth and Decay of Perturbations at an Interface in a Stagnation Counterflow," J. Fluid Mech. 84, pp. 401-409.

45. Pilch, M. M., Allen M. D., and Klamerus E. W., “Resolution of the Direct Containment Heating Issue for All Westinghouse Plants With Large Dry Containments or Subatmospheric containments,” NUREG/CR-6338, SAND95-2381, Sandia National Laboratories, Feb. 1996.